Journal of Materials Chemistry A

Carbon nanotube-linked hollow carbon nanospheres doped with iron and nitrogen as single-atom catalysts for oxygen reduction reaction in acidic solutions

Journal:	*Journal of Materials Chemistry A*
Manuscript ID	TA-CMT-01-2019-000508.R1
Article Type:	Communication
Date Submitted by the Author:	30-Apr-2019
Complete List of Authors:	Li, Jin-Cheng; Fok Ying Tung Research Institute, Hong Kong University of Science and Technology; Washington State University Cheng, Min; Institute of Metal Research, Chinese Academy of Sciences, Shenyang National Laboratory for Materials Science, Li, Tao; Argonne National Lab, Ma, Lu; Argonne National Laboratory, Ruan, Xiaofan; Washington State University, School of Mechanical and Materials Engineering Liu, Dong; Washington State University Cheng, Hui-Ming; Institute of Metal Research, CAS, Advanced Carbon Divisioin, SYNL; Tsinghua-Berkeley Shenzhen Institute, Liu, Chang; Institute of Metal Research, Chinese Academy of Sciences, Advanced Carbon Divisioin,Shenyang National Laboratory for Materials Science Du, Dan; Washington State University, School of Mechanical and Materials Engineering Wei, Zidong; Chongqing university, chemistry Lin, Yuehe; Washington State University, School of Mechanical and Materials Engineering Shao, Minhua; The Hong Kong University of Science and Technology, Chemical and Biomolecular Engineering

Journal Name

COMMUNICATION

Carbon nanotube-linked hollow carbon nanospheres doped with iron and nitrogen as single-atom catalysts for oxygen reduction reaction in acidic solutions

Received 00th January 20xx,
Accepted 00th January 20xx

DOI: 10.1039/x0xx00000x

www.rsc.org/

Jin-Cheng Li,[a, b, c] Min Cheng,[c] Tao Li,[d, e] Lu Ma,[d] Xiaofan Ruan,[b] Dong Liu,[b] Hui-Ming Cheng,[c] Chang Liu,*[c] Dan Du,[b] Zidong Wei,[f] Yuehe Lin *[b] and Minhua Shao *[a, g]

Non-noble metal electrocatalysts toward oxygen reduction reaction (ORR) are highly required to substitute expensive Pt/C in the cathode of proton exchange membrane fuel cells. However, the relatively low ORR activity of these Pt-free catalysts under acidic conditions is the major issue. Herein, we engineered a three-dimensional structure consisting of atomically dispersed Fe, N-doped hollow carbon nanospheres linked by carbon nanotubes as electrocatalyst for the ORR. Benefiting from the unique structure and high-density atomic Fe-N_x sites, this new type of electrocatalyst showed an impressively ORR half-wave potential of 0.84 V and kinetic current density of 13.1 mA cm^{-2} at the potential of 0.8 V in acidic media, which was even better that commercial Pt/C.

Proton exchange membrane fuel cells (PEMFCs) have attracted great interest owing to their high energy density and zero emission.[1-3] However, their wide applications are restricted by their high cost. About 50% of the total cost of a PEMFC stack is attributed to noble-metal catalysts, most of which are employed to improve the oxygen reduction reaction (ORR) kinetics at the cathode.[4-6] Thus, considerable efforts and resources have been devoted to exploring inexpensive noble-metal-free ORR catalysts in recent years.[7-9]

As a type of noble-metal-free electrocatalysts, Fe-N-C materials have attracted great attention.[10-14] Such materials are usually prepared by pyrolyzing organic precursors containing Fe, N and C sources at high temperatures. Single Fe atoms coordinated by N doping (Fe-N_x) sites in the surface have been suggested to be as active as Pt.[15, 16] However, the ORR performance of current Fe-N-C materials is still inferior to Pt, especially in acidic conditions. Increasing the density of Fe-N_x sites is an effective strategy to further improve the ORR performance. Since Fe atoms are mobile and tend to agglomeration to form inactive nanosized compounds during the high-temperature treatment, simply increasing Fe content in the precursors is ineffective.[17, 18] Recently, some more effective strategies including silica layer protecting[19], template assisting[20], ionothermal stabilizing[21], and spatially confining[22] were applied to synthesize Fe-N-C materials enriched with atomic Fe-N_x sites (denoted as single-atom Fe catalysts). These single-atom Fe catalysts hold excellent ORR activities in alkaline conditions, but their ORR activities in acidic media are still less than satisfactory.

Conducting polymers such as polyaniline and polypyrrole have been widely employed as precursors for the preparation of Fe-N-C materials because of their low cost, high N content, and uniform N distribution.[23-25] Such N groups in conducting polymers are able to adsorb and anchor Fe ions, leading to well dispersive Fe atoms in the precursors and beneficial to the formation of atomic Fe-N_x sites. However, the Fe-N-C materials prepared by directly pyrolyzing conducting polymer-based precursors are suffered from poor electrical conductivity and undesirable architecture, which are prejudicial to electron transfer and mass transport processes involved in the ORR.[25] Furthermore, the number of accessible active sites is also limited.

Here, we designed and synthesized three-dimensional Fe, N-doped hollow carbon nanospheres linked by carbon nanotubes (CNT-Fe/NHCNS). CNT-linked hollow polymer nanospheres composite was synthesized by self-assembly polymerization of aniline and pyrrole in the presence of CNTs. In combination with atom isolating technique involving Fe^{3+}/Na^+ adsorption and pyrolysis, high-density of single Fe atoms anchored in N-doped hollow carbon nanospheres were achieved, which was confirmed by atomically scaled annular dark-field scanning transmission electron microscopy (ADF-STEM) imaging and extended X-ray absorption fine structure (EXAFS). Benefiting

[a] Fok Ying Tung Research Institute, Hong Kong University of Science and Technology, Guangzhou 511458, China.
[b] School of Mechanical and Materials Engineering, Washington State University, Pullman, WA 99164, USA.
[c] Shenyang National Laboratory for Materials Science, Institute of Metal Research, Chinese Academy of Sciences, Shenyang 110016, China.
[d] Department of Chemistry and Biochemistry, Northern Illinois University, 1425 W. Lincoln Hwy., DeKalb, IL, 60115, USA.
[e] X-ray Science Division, Argonne National Laboratory, 9700 South Cass Avenue, Lemont, Illinois 60439, United States.
[f] College of Chemistry and Chemical Engineering, Chongqing University, Chongqing, 400044, China.
[g] Department of Chemical and Biological Engineering, Hong Kong University of Science and Technology, Clear Water Bay, Kowloon, Hong Kong, China.
*Email kemshao@ust.hk, minhua@gmail.com
The manuscript was written through contributions of all authors. All authors have given approval to the final version of the manuscript.
Electronic Supplementary Information (ESI) available: [details of any supplementary information available should be included here]. See DOI: 10.1039/x0xx00000x

from the characteristic of highly electrical conductivity of CNTs, three-dimensional porous architecture and high-density of atomic Fe-N_x sites, the CNT-Fe/NHCNS showed excellent ORR performance in acidic media.

Figure 1a shows the scheme of the preparation process of CNT-Fe/N-HCNS, which involves three steps including chemical self-assembly, metal cation adsorption, and high-temperature pyrolysis. Before the synthesis, CNTs were subjected to the mixed nitric/sulfuric acid treatment to improve the dispersity in aqueous solution and remove nanosized Fe species left during the CNT growth. The CNTs experienced the above treatment still remain their structure intact (Figure S1). After a high-temperature treatment at 900˚C, the surface oxygenic functional groups were removed resulting in a high electrical conductivity.[26-28] To carry out the chemical self-assembly, the obtained functionalized CNTs were dispersed into a polyvinyl pyrrolidone solution. Aniline and pyrrole monomers were added into the above mixture under continuous stirring in an ice bath. Ammonium peroxydisulfate was then added to induce self-assembly polymerization of aniline and pyrrole, leading to formation of CNT-linked hollow polymer nanospheres. Subsequently, the above product was dispersed in a mixture of iron nitrate and sodium chloride to adsorb metal cations. Finally, the precursor with adsorbates was undergone a typical three-step process of pyrolysis under N_2, acid leaching and NH_3 activation, to obtain CNT-Fe/N-HCNS.[24] According to previous report, the introduced isolating agents could effectively suppress Fe agglomeration and conduce to achieve active atomic Fe-N_x sites.[29] Herein, sodium chloride was employed as an isolating agent to obtain a high density of atomic Fe-N_x active sites, which is significant for acquiring highly efficient ORR performance.

Previous reports have verified that pyrolysis temperature plays an essential role in achieving highly active Fe-N-C catalysts. A low temperature can result in low graphitization and poor electrical conductivity, while a high temperature can lead to high electrical conductivity as well as formation of inactive nanosized Fe species rather than enrichment of atomic Fe-N_x sites.[30, 31] Accordingly, we first evaluated the ORR activities of the CNT-Fe/NHCNS materials in an acidic solution as a function of heat-treatment temperature in the range of 800-1000°C. As show in Figure S2, the rotating ring-disk electrode (RRDE) measurements shows that CNT-Fe/NHCNS material prepared at 900 °C exhibits the best ORR activity, which was disclosed by the important performance evaluation parameters of half-wave potential, limiting current density, H_2O_2 yield, and electron transfer number. Thus, this sample was chosen for further characterization and discussion.

The morphology and structure of CNT-Fe/NHCNS were characterized by scanning electron microscopy (SEM) and transmission electron microscopy (TEM). Figure 1b-c show typical SEM and TEM images of CNT-Fe/NHCNS. There are abundant carbon nanospheres with a diameter around 130 nm. Interestingly, carbon nanospheres are linked through the CNTs, like tomatoes on sticks. Such structure can shorten the electron transport pathway between the carbon nanospheres and accelerate the electron transfer. The carbon nanospheres have a hollow structure, which increases the surface area and number of active sites exposed to electrolyte. The hollow carbon nanospheres hold a porous structure consisting of crooked few-layer graphene (Figure 1d and Figure S3a). The CNT surface is coated with a thin carbon layer (Figure S3b). No nanoparticle was detected in hollow carbon nanospheres, suggesting that Fe might be hosted in an isolated atomic form. Nevertheless, there are still a small amount of nanosized Fe species buried in the CNT inner chamber (Figure S4a). These particles survived from the acidic treatment of CNTs seem to have no effect on the formation of atomic Fe-N_x moieties in outer carbon layers (Figure S4b). Figure S5 shows CNT-Fe/NHCNS has a hierarchically porous structure. The Brunauer-Emmett-Teller (BET) surface area and electrochemically accessible surface area (Sa) were as large as 897 $m^2 g^{-1}$ and 565 $m^2 g^{-1}$, respectively. Such structural features are favorable to the ORR. Raman spectroscopy was performed to further characterize the crystallinity of CNT-Fe/NHCNS. As shown in Figure S6, the line shapes of the G-band and D-band peak of CNT-Fe/NHCNS are similar to those of CNTs. Furthermore, the intensity ratio of G-band to D-band of CNT-Fe/NHCNS is 0.78, close to that of CNTs (0.82). These results further confirm that CNT-Fe/NHCNS has a high crystallinity, which endows it with fast electron transfer capacity.

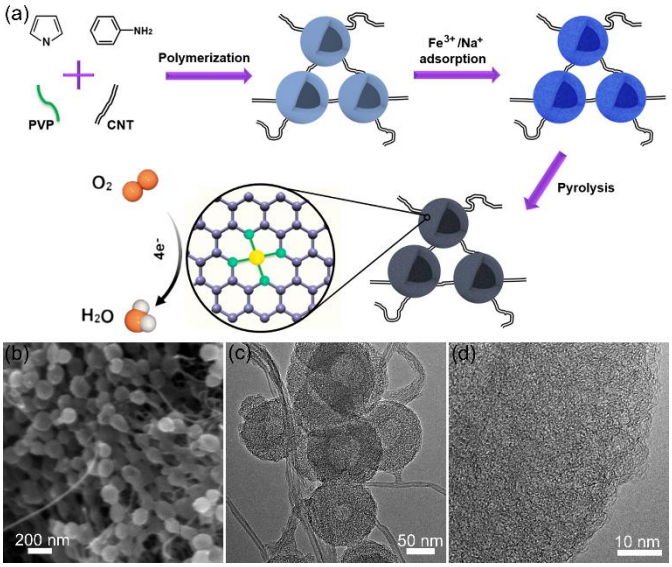

Figure 1. Schematic illustration of the synthesis process of CNT-Fe/NHCNS for the ORR. (b) SEM image, (c) low-magnification TEM, and (d) high-magnification TEM image of CNT-Fe/NHCNS.

Figure 2a shows the X-ray diffraction pattern of CNT-Fe/NHCNS. There are two characteristic peaks of graphitic carbon at 25.4° for the (002) plane and 43.4° for the (101) plane, which further demonstrates that CNT-Fe/NHCNS has a good crystallinity. Furthermore, no diffraction peak from Fe species was detected. We carried out aberration-corrected scanning TEM to identify single Fe atoms CNT-Fe/NHCNS. Owing to a large atomic number difference between Fe and C, the Z-contrast imaging can effectively identify Fe distribution at the atomic level. As illustrated in Figure 2b, dense isolated Fe atoms (bright dots) exist in CNT-Fe/NHCNS. To further confirm the Fe configurations in CNT-Fe/NHCNS at the atomic level, X-ray absorption near-edge structure (XANES) and EXAFS were performed. Figure 2c shows the Fe K-edge XANES spectra of CNT-Fe/NHCNS and reference samples of Fe foil, FeO and Fe_2O_3. Clearly, the near-edge absorption energy of CNT-Fe/NHCNS is between those of bi- (FeO) and trivalent (Fe_2O_3) iron, indicating the Fe oxidation state of Fe-N_x in CNT-Fe/NHCNS is between 2+ and 3+, consistent

with X-ray photoelectron spectroscopy (XPS) results (Figure S7) and well in line with previous reported single-atom Fe catalysts.[32] Fourier-transform EXAFS curve of CNT-Fe/NHCNS presents a main Fe-N peak at 1.4 Å (Figure 2d), further revealing that majority of Fe atoms are atomically isolated in hollow carbon nanospheres and carbon layer on CNTs. A weak shoulder at 2.1 Å was also detected, which may originate from nanosized Fe species buried in the inner chamber of CNTs, in agreement with TEM results (Figure S4). According to the fitting parameters given in Table S1, the coordination number is 4.45±1.23. All the above characterization results demonstrate that CNT-Fe/NHCNS has a unique structure and high-density atomic Fe-N_x active sites.

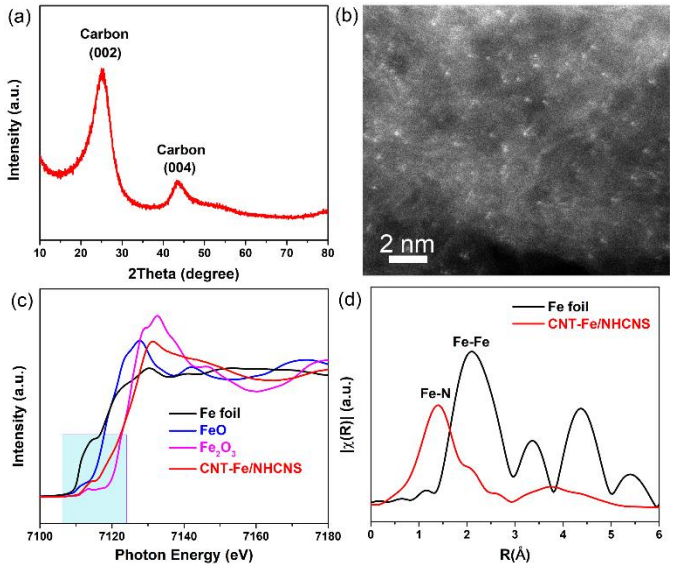

Figure 2. (a) XRD pattern of CNT-Fe/NHCNS. (b) ADF-STEM image of CNT-Fe/NHCNS. (c) Fe K-edge XANES spectra of Fe foil, FeO, Fe_2O_3, and CNT-Fe/NHCNS. (d) Fourier-transform EXAFS spectra of Fe foil and CNT-Fe/NHCNS.

To evaluate the ORR catalytic activity of CNT-Fe/NHCNS, RRDE and rotating disk electrode (RDE) evaluation were carried out in an O_2-saturated 0.1 M $HClO_4$ solution. Figure 3a shows the disk electrode polarization curves of CNT-Fe/NHCNS (loading: 0.2 mg cm^{-2}) and Pt/C (20 wt% Pt, loading: 0.1 mg cm^{-2}). Clearly, both CNT-Fe/NHCNS and Pt/C have a stable diffusion-limiting current density platform, while CNT-Fe/NHCNS holds a limiting current density of ~6.0 mA cm^{-2}, larger than that of Pt/C (~5.4 mA cm^{-2}). More importantly, the half-wave potential of CNT-Fe/NHCNS reaches 0.84 V, identical to that of Pt/C and much better than those of recently reported representative single-atom Fe catalysts (0.78-0.82 V).[19, 29, 33, 34] The H_2O_2 yield at the whole potentials is below 4% and the mean value is ~2%, bearing comparison with those of Pt/C (Figure 3b). Such a low H_2O_2 yield reveals that CNT-Fe/NHCNS has a high ORR catalytic efficiency in acidic media. The electron transfer number of CNT-Fe/NHCNS derived from disk/ring currents is in the range of 3.93 to 3.98 in the whole potential range, suggesting a highly efficient four-electron-transfer pathway. Furthermore, RDE measurements in combination with Koutecky-Levich (K-L) equation calculations exhibit the electron transfer number of CNT-Fe/NHCNS is ~4.0 (Figure S8), which further reveals its ORR catalytic mechanism following a highly efficient four-electron-transfer pathway. Figure 3c shows the Tafel curves deduced from the polarization curves in Figure 3a on the basis of the mass transport correction. CNT-Fe/NHCNS holds a smaller Tafel slope compared to Pt/C (67 mV/decade versus 76 mV/decade), which reveals that CNT-Fe/NHCNS holds a better ORR kinetics.[35] Furthermore, CNT-Fe/NHCNS has an impressive kinetic current density of 13.1 mA cm^{-2} at 0.8 V, larger than that of Pt/C (10.2 mA cm^{-2}). Based on the above results, the acidic activity of CNT-Fe/NHCNS for the ORR is demonstrated to be superior to Pt/C. Furthermore, to preliminarily evaluate the intrinsic activity of Fe-N_x in CNT-Fe/NHCNS, turn-over frequency (TOF, number of electrons reduced per Fe-N_x active site and per second at 0.8 V) was deduced from kinetic current density and Fe content (2.18 wt.% from ICP-MS). The average TOF was as large as 1.74 (e^- $site^{-1}$ s^{-1}), which is larger than typically reported Fe-N-C catalysts (Table S2). Except for the catalytic activity, the stability is also a key factor in assessing a practical ORR electrocatalyst. Figure 3d shows the ORR polarization curves of CNT-Fe/NHCNS before and after potential cycles between 0.7 and 1.1 V at 50 mV s^{-1}. After 5000 continuous cycles, the half-wave potential of CNT-Fe/NHCNS showed a small negative shift of ~15 mV, which was comparable to that of Pt/C (13 mV, Figure S9).

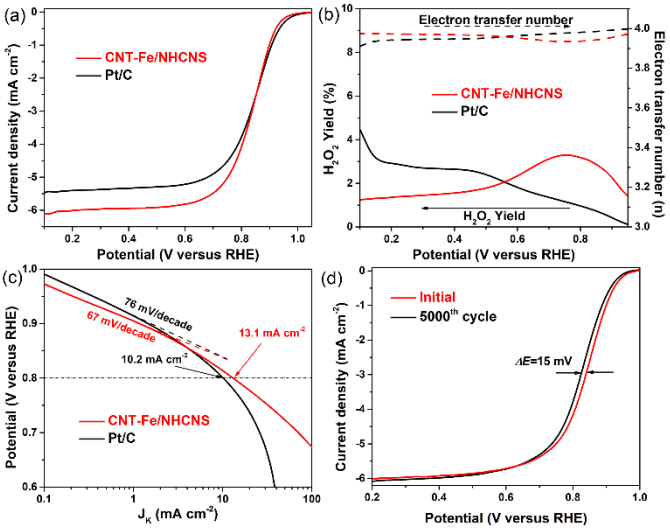

Figure 3. (a) ORR polarization curves, (b) H_2O_2 yield and electron transfer number, and (c) Tafel plots of CNT-Fe/NHCNS with a loading of 0.2 mg cm^{-2} and Pt/C with a loading of 0.1 mg cm^{-2}. (d) ORR polarization curves of CNT-Fe/NHCNS before and after 5000 potential cycles.

The highly efficient ORR performance of CNT-Fe/NHCNS can be attributed to the three-dimensional nanostructure of CNT-linked carbon nanospheres and high-density atomic Fe-N_x active sites. To better understand the role of the structure and Fe on the ORR activities, control experiments were conducted: (1) single Fe atoms were anchored on isolated N-doped hollow carbon nanospheres (Fe/NHCNS) only without introduction of CNTs; (2) three-dimensional nanostructure of CNT linked N-doped hollow carbon nanospheres (CNT-NHCNS) only without introduction of Fe. Figure 4a compares the ORR polarization curves of CNT-Fe/NHCNS, CNT-NHCNS, and Fe/NHCNS. Compared to CNT-NHCNS, CNT-Fe/NHCNS has a substantial improvement for the ORR, which is revealed by its

remarkably more positive half-wave potential (0.84 V versus 0.69 V), a much lower H_2O_2 yield (Figure S10), and a considerably larger kinetic current density (Figure S11). XPS was applied to detect chemical compositions of these carbon materials and the results are shown in Figure 4b. As expected, no Fe signal was detected in CNT-NHCNS. By contrast, the Fe contents in CNT-Fe/NHCNS and Fe/NHCNS are both ~0.3 at.%. Furthermore, although N content in CNT-NHCNS is slightly higher than that in CNT-Fe/NHCNS (Figure 4b), the percentage of defective N configurations (pyridinic and pyrrolic N), acknowledged as coordination sites for single Fe atoms, is obviously lower (Figure 4c). Consequently, atomic Fe-N_x sites are demonstrated as the critical factor for achieving high ORR activity. In the sample without introducing CNTs (Fe/NHCNS), the N content and configuration are almost identical to those of CNT-Fe/NHCNS (Figure 4c, d). This result suggests that like CNT-Fe/NHCNS, Fe/NHCNS is also enriched with atomic Fe-N_x active sites. Interestingly, Fe/NHCNS has a distinct negative shift of the half-wave potential (Figure 4a) and the kinetic current density of Fe/NHCNS at 0.8 V is only half of that of CNT-Fe/NHCNS (Figure S11), although the onset potentials of CNT-Fe/NHCNS and Fe/NHCNS are almost the same. That is, the ORR onset potential is mainly determined by the nature of active sites. Nevertheless, the ORR involves multi-step electron transfer.[36-38] The addition of CNTs in CNT-Fe/NHCNS can couple with isolated carbon nanospheres with Fe-N_x active sites and accelerate the electron transfer, which is revealed by larger current densities. To reveal the role of conductivity improvement contributed by CNTs, electrochemical impedance spectra measurements were carried out to directly measure the electrical conductivity of Fe/NHCNS and CNT-Fe/NHCNS. As shown in Figure S12a, the CNT-Fe/NHCNS sample possesses a resistance of 3.8 Ω, much lower than that of Fe/NHCNS without CNTs (14.7 Ω). This result demonstrates that atomically dispersed Fe, N-doped hollow carbon nanospheres linked by CNTs can indeed improve the electrical conductivity. In addition, thermogravimetry was performed to evaluate the crystallinity of Fe/NHCNS and CNT-Fe/NHCNS. Figure S12b shows CNT-Fe/NHCNS has much higher oxidation resistance temperature than that of Fe/NHCNS, suggesting CNT-Fe/NHCNS possesses higher graphitization and better electrical conductivity, in good agreement with electrochemical impedance spectra result.

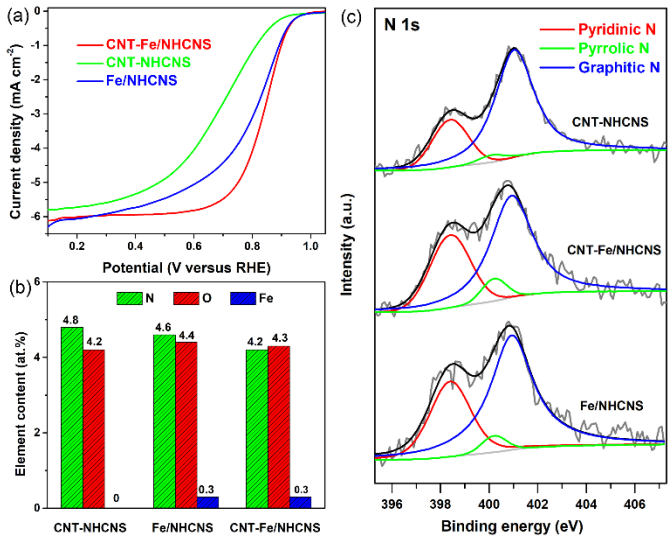

Figure 4. (a) ORR polarization curves of CNT-Fe/NHCNS, CNT-NHCNS, and Fe/NHCNS with the same loading of 0.2 mg cm^{-2}. (b) Chart showing N, O, and Fe contents in CNT-Fe/NHCNS, CNT-NHCNS, and Fe/NHCNS measured by XPS technique. (c) High-resolution N 1s spectra of CNT-Fe/NHCNS, CNT-NHCNS, and Fe/NHCNS.

Conclusions

In summary, we engineered and synthesized a three-dimensional architecture of Fe, N-doped hollow carbon nanospheres linked by CNTs. Aberration-corrected TEM and EXAFS characterization results demonstrated that the nanocomposite was enriched with atomic Fe-N_x active sites. Benefiting from its unique structure and high-density of atomic Fe-N_x active sites, the catalyst showed excellent ORR activity with a half-wave potential of 0.84 V and kinetic current density of 13.1 mA cm^{-2} at the potential of 0.8 V in acidic media, which is even better than those of the commercial Pt/C catalyst. Furthermore, control experiments demonstrated that CNTs can couple with isolated Fe-N_x modified carbon nanospheres and accelerate the electron transfer, leading to better ORR performance.

Conflicts of interest

The authors declare no competing financial interest.

Notes and references

1. D. Banham and S. Ye, *ACS Energy Lett.*, 2017, DOI: 10.1021/acsenergylett.6b00644, 629-638.
2. Z. Chen, D. Higgins, A. Yu, L. Zhang and J. Zhang, *Energy Environ. Sci.*, 2011, **4**, 3167-3192.
3. F. Jaouen, E. Proietti, M. Lefevre, R. Chenitz, J.-P. Dodelet, G. Wu, H. T. Chung, C. M. Johnston and P. Zelenay, *Energy Environ. Sci.*, 2011, **4**, 114-130.
4. M. Shao, Q. Chang, J.-P. Dodelet and R. Chenitz, *Chem. Rev.*, 2016, **116**, 3594–3657.
5. J.-C. Li, Z. Wei, D. Liu, D. Du, Y. Lin and M. Shao, Top. Curr. Chem., 2019, **377**, 4.
6. H. Zhang, S. Hwang, M. Wang, Z. Feng, S. Karakalos, L. Luo, Z. Qiao, X. Xie, C. Wang, D. Su, Y. Shao and G. Wu, *J. Am. Chem. Soc.*, 2017, **139**, 14143–14149.
7. B. Y. Guan, L. Yu and X. W. Lou, *Energy Environ. Sci.*, 2016, **9**, 3092-3096.
8. J. Li, S. Ghoshal, W. Liang, M.-T. Sougrati, F. Jaouen, B. Halevi, S. McKinney, G. McCool, C. Ma, X. Yuan, Z.-F. Ma, S. Mukerjee and Q. Jia, *Energy Environ. Sci.*, 2016, **9**, 2418-2432.
9. J.-C. Li, P.-X. Hou, S.-Y. Zhao, C. Liu, D.-M. Tang, M. Cheng, F. Zhang and H.-M. Cheng, *Energy Environ. Sci.*, 2016, **9**, 3079-3084.
10. S. Gadipelli, T. Zhao, S. A. Shevlin and Z. Guo, *Energy Environ. Sci.*, 2016, **9**, 1661-1667.
11. D. Higgins, P. Zamani, A. Yu and Z. Chen, *Energy Environ. Sci.*, 2016, **9**, 357-390.
12. S. H. Noh, M. H. Seo, J. Kang, T. Okajima, B. Han and T. Ohsaka, *NPG Asia Mater*, 2016, **8**, e312.
13. Y. Zheng, Y. Jiao, Y. Zhu, Q. Cai, A. Vasileff, L. H. Li, Y. Han, Y. Chen and S.-Z. Qiao, *J. Am. Chem. Soc.*, 2017, **139**, 3336–3339.
14. A. Han, W. Chen, S. Zhang, M. Zhang, Y. Han, J. Zhang, S. Ji, L. Zheng, Y. Wang, L. Gu, C. Chen, Q. Peng, D. Wang and Y. Li, *Adv. Mater.*, 2018, **30**, 1706508.

15. W.-J. Jiang, L. Gu, L. Li, Y. Zhang, X. Zhang, L.-J. Zhang, J.-Q. Wang, J.-S. Hu, Z. Wei and L.-J. Wan, *J. Am. Chem. Soc.*, 2016, **138**, 3570-3578.
16. S. Kattel and G. Wang, *J. Phys. Chem. Lett.*, 2014, **5**, 452-456.
17. J. Li, Y. Song, G. Zhang, H. Liu, Y. Wang, S. Sun and X. Guo, *Adv. Funct. Mater.*, 2017, **27**, 1604356.
18. Q. Lai, L. Zheng, Y. Liang, J. He, J. Zhao and J. Chen, *ACS Catal.*, 2017, DOI: 10.1021/acscatal.6b02966, 1655-1663.
19. Y. J. Sa, D.-J. Seo, J. Woo, J. T. Lim, J. Y. Cheon, S. Y. Yang, J. M. Lee, D. Kang, T. J. Shin, H. S. Shin, H. Y. Jeong, C. S. Kim, M. G. Kim, T.-Y. Kim and S. H. Joo, *J. Am. Chem. Soc.*, 2016, **138**, 15046–15056.
20. Y. Han, Y.-G. Wang, W. Chen, R. Xu, L. Zheng, J. Zhang, J. Luo, R.-A. Shen, Y. Zhu, W.-C. Cheong, C. Chen, Q. Peng, D. Wang and Y. Li, *J. Am. Chem. Soc.*, 2017, **139**, 17269-17272.
21. J.-D. Yi, R. Xu, Q. Wu, T. Zhang, K.-T. Zang, J. Luo, Y.-L. Liang, Y.-B. Huang and R. Cao, *ACS Energy Lett.*, 2018, **3**, 883-889.
22. W. Zhang, X. Xu, C. Zhang, Z. Yu, Y. Zhou, Y. Tang, P. Wu and S. Guo, *Small Methods*, 2017, **1**, 1700167.
23. J.-C. Li, S.-Y. Zhao, P.-X. Hou, R.-P. Fang, C. Liu, J. Liang, J. Luan, X.-Y. Shan and H.-M. Cheng, *Nanoscale*, 2015, **7**, 19201-19206.
24. G. Wu, K. L. More, C. M. Johnston and P. Zelenay, *Science*, 2011, **332**, 443-447.
25. K. Yuan, S. Sfaelou, M. Qiu, D. Lützenkirchen-Hecht, X. Zhuang, Y. Chen, C. Yuan, X. Feng and U. Scherf, *ACS Energy Lett.*, 2018, **3**, 252-260.
26. J.-C. Li, D.-M. Tang, P.-X. Hou, G.-X. Li, M. Cheng, C. Liu and H.-M. Cheng, *MRS Commun.*, 2018, **8**, 1158-1166
27. Y. Liu, F. Chen, W. Ye, M. Zeng, N. Han, F. Zhao, X. Wang and Y. Li, *Adv. Funct. Mater.*, 2017, **27**, 1606034
28. S. Yasuda, A. Furuya, Y. Uchibori, J. Kim and K. Murakoshi, *Adv. Funct. Mater.*, 2016, **26**, 738-744.
29. J.-C. Li, Z.-Q. Yang, D.-M. Tang, L. Zhang, P.-X. Hou, S.-Y. Zhao, C. Liu, M. Cheng, G.-X. Li, F. Zhang and H.-M. Cheng, *NPG Asia Mater*, 2018, **10**, e461.
30. J. Li, J. Chen, H. Wang, Y. Ren, K. Liu, Y. Tang and M. Shao, *Energy Storage Mater.*, 2017, **8**, 49-58.
31. B.-C. Hu, Z.-Y. Wu, S.-Q. Chu, H.-W. Zhu, H.-W. Liang, J. Zhang and S.-H. Yu, *Energy Environ. Sci.*, 2018, **11**, 2208-2215.
32. S. Fu, C. Zhu, D. Su, J. Song, S. Yao, S. Feng, M. H. Engelhard, D. Du and Y. Lin, *Small*, 2018, **14**, 1703118.
33. Y. Chen, S. Ji, Y. Wang, J. Dong, W. Chen, Z. Li, R. Shen, L. Zheng, Z. Zhuang, D. Wang and Y. Li, *Angew. Chem. Int. Ed.*, 2017, **56**, 6937–6941
34. C. Zhang, Y.-C. Wang, B. An, R. Huang, C. Wang, Z. Zhou and W. Lin, *Adv. Mater.*, 2017, **29**, 1604556.
35. J.-C. Li, P.-X. Hou, M. Cheng, C. Liu, H.-M. Cheng and M. Shao, *Carbon*, 2018, **139**, 156-163.
36. A. Kulkarni, S. Siahrostami, A. Patel and J. K. Nørskov, *Chem. Rev.*, 2018, **118**, 2302–2312.
37. J.-C. Li, P.-X. Hou and C. Liu, *Small*, 2017, **13**, 1702002
38. Y. P. Zhu, C. Guo, Y. Zheng and S.-Z. Qiao, *Acc. Chem. Res.*, 2017, **50**, 915–923.

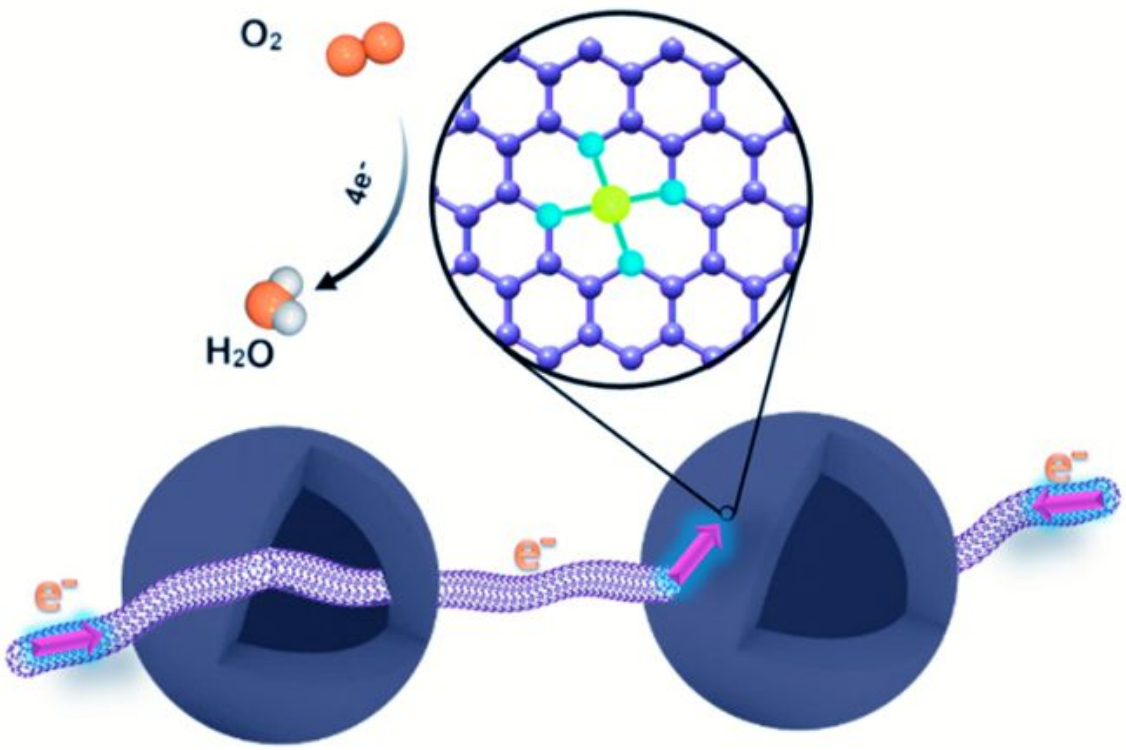

A three-dimensional structure consisting of atomically dispersed Fe, N-doped hollow carbon nanospheres linked by carbon nanotubes was engineered as electrocatalyst showing highly efficient oxygen reduction activity in acidic conditions